Cover Sheet

This is a preprint of a manuscript that is currently undergoing peer review. Subsequent versions of the manuscript may have different content. It has been written and published here to share experience and receive feedback. We invite you to contact us directly.

Xuewei Wang (xuewei.wang@unc.edu)
Angel Hsu (angel.hsu@unc.edu)
T.C. Chakraborty (tc.chakraborty@pnnl.gov)

Citizen and Machine Learning-aided high-resolution mapping of urban heat exposure and stress

Xuewei Wang[1,2,3], Angel Hsu[1,2,3], TC Chakraborty[4]
[1]Data-Driven EnviroLab, University of North Carolina at Chapel Hill, United States
[2]Department of Public Policy, University of North Carolina at Chapel Hill, United States
[3]Institute for Environment, University of North Carolina at Chapel Hill, United States
[4]Atmospheric Sciences & Global Change Division, Pacific Northwest National Laboratory, United States

Abstract

Through conversion of land cover to more built-up, impervious surfaces, cities are creating hotter environments for urban residents. Existing measurements of heat and heat stress, however, are often insufficient to capture intra-urban variability of exposure. This study provides a replicable method for modeling air temperature, humidity, and heat stress over an urban area, engaging citizens in collecting high-temporal and spatially-resolved air temperature and humidity measurements. We use low-cost, consumer-grade sensors combined with satellite remote sensing data and machine learning to map urban air temperature and humidity over various land-cover classes to understand intra-urban spatial variability of heat at a relatively high resolution (10 meters). Our findings show that individuals may be exposed to higher levels of heat and heat stress than weather station data suggest, and this heat varies according to land cover type, with tree-covered land the coolest and built-up areas the warmest, and time of day, with higher temperatures observed during the early afternoon. Combining our resulting dataset with sociodemographic data, we find an inverse relationship between income and our heat metrics, although the sensitivity of this relationship varies depending on which metric is used. Policymakers and urban planners can use this data to identify areas exposed to high heat and heat stress as a first step to design effective mitigation measures.

Introduction

Extreme heat in urban areas is becoming a critical public health concern. During 2018-2020, a total of 3,066 heat-related deaths occurred in the United States ("QuickStats," 2022). Climate change is increasing the probability of intense, prolonged heat waves in many parts of the world (IPCC, 2021; Vargas Zeppetello et al., 2022). The urban heat island effect, the phenomenon of higher temperatures in urban areas compared to their rural surroundings (Oke, 1982), exacerbates the negative health effects of heat waves and extreme temperatures within cities. Exposure to excessive heat can kill people, and it can also cause general discomfort, respiratory problems, heat cramps and exhaustion, non-fatal heat strokes, and dehydration (Heal & Park, 2016; Park et al., 2020; Zander et al., 2015). At the population level, extreme heat can lead to a loss of labor productivity and decreased learning (Tan et al., 2010). These cumulative impacts are expected to increase in frequency and severity as the portion of the human population living in cities is projected to grow over the next few decades and climate change worsens (Ritchie & Roser, 2018). The IPCC Sixth Assessment Report on Climate Change anticipates increases in the frequency and intensity of heat waves, with pernicious effects that interact dynamically with urban heat exposure (Krayenhoff et al., 2018). Future urbanization is also expected to worsen average summer daytime and daytime temperatures of 0.5 °C–0.7 °C and up to∼3 °C in some locations (Huang et al., 2021).

Within cities, prior research has shown temperatures vary considerably according to multiple factors. The presence (or absence) of urban green space, amount (size of city), form (building height, ratio of building height to width of street canyon, etc.), and color (influencing reflectivity of solar radiation) of built-up structures, and intensity of human activity (through increased anthropogenic heat flux) all lead to intra-urban variability of temperatures and the urban heat island effect (Benz & Burney, 2021; T. Chakraborty et al., 2019). Since urban landscapes are diverse and thermally complex, heat is unevenly distributed (Shi et al., 2021), and research has shown differential access to green space and tree cover along with exposure to denser, built-up urban areas translates into varying heat exposure (T. Chakraborty et al., 2019, 2020; Ziter et al., 2019). These temperature disparities also affect different sociodemographic groups in different ways, with people of color and those living below the poverty line found to be systematically exposed to higher temperatures than non-Hispanic white and wealthy counterparts in nearly all major U.S. cities (Benz & Burney, 2021; Hsu et al., 2021).

Despite the increasing severity and probability of heat waves and extreme heat waves disproportionately impacting urban areas, high-resolution measurements attuned to measure intra-urban heat variability, or what is often referred to as the urban heat archipelago (Muller et al., 2013; Ziter et al., 2019) effect, are lacking for most cities. Temperature and weather data for an entire city are often based on one or a few meteorological stations at best, which are fixed either at a city's center or near an airport, which mean they do not characterize an entire city (van Hove et al., 2015). Therefore, most studies on heat-related mortality and morbidity utilizing these single-point weather station measurements make a critical limiting assumption that all people living in a geographic area are all exposed similarly (Rajagopalan et al., 2020). To address this limitation, researchers have turned to collecting ground-based data (i.e., air temperature, humidity, etc.), which can be time and resource consuming, or using satellite remote sensing data. Satellite measurements have the advantage of inexpensively providing data using consistent methods at high frequency and at policy-relevant geographic scales (Benz & Burney, 2021; T. Chakraborty et al., 2020; Hoffman et al., 2020; Hsu et al., 2021). Of the factors that pertain to urban heat and are of interest from a public health perspective, however, satellites only measure radiometric land surface temperature (LST) (e.g., Manoli et al., 2019, 2020; Zhao et al., 2014) - a significant limitation since this measurement is difficult to apply to pedestrian-level heat exposure. In addition, satellite data are limited to certain times of the day (i.e., overpass times), cloud cover, and the view angle (Shi et al., 2021). Studies have also found weak relationships between satellite-derived LST and heat stress (TChakraborty et al., 2022).

To address these data limitations, citizen science methods, which engage local communities in collecting relevant data such as temperature and humidity at a high temporal and spatial resolution, have been proposed as possible solutions to provide more detailed data to improve estimates of intra-urban temperature variation. Since 2017, the National Oceanic and Atmospheric Administration (NOAA) has partnered with nearly 50 cities in the U.S. to design heat mapping campaigns that utilize mobile sensors attached to vehicles to map intra-urban heat variability throughout a typically hot summer day (NOAA, n.d.). These data have been used to develop city-wide heat maps (Shandas et al., 2019) and inform local policy regarding heat mitigation measures. Although these campaigns provide baseline measures of intra-urban heat variability for participating cities, Shi et al., 2021 compared the NOAA citizen heat mapping data collected in Baltimore in 2019 to fixed sensor data and found several limitations, including the need for temperatures above land surfaces other than roads collected through either bicycle or on-foot traverses.

Recent advances in machine learning (ML) and other non-linear, non-parametric statistical modeling approaches provide potential to combine earth observation data along with ground-based measurements to develop more comprehensive and higher-resolution, continuous maps of heat exposure and stress across an urban area. Several previous studies have combined satellite remote imagery along with ground-based measurements, either citizen-collected data (Shandas et al., 2019), weather stations (Ho et al., 2014; Venter et al., 2020), or sensors (Zumwald et al., 2021), using random forest regression, a non-parametric ML technique for classification and regression modeling to predict and evaluate ambient air temperature in three U.S. cities. None of these studies, however, predict humidity, which is an important contributor to human thermal comfort (Steeneveld et al., 2011).

In this study, we provide a replicable, scalable approach to engaging citizens in utilizing low-cost, consumer-grade, hand-held sensors to map varied land-cover traverses of intra-urban heat, humidity, and heat stress variability. Combined with satellite remote sensing data on land cover, normalized difference vegetation index or NDVI (a measure of greenness), normalized difference built-up index or NDBI (a proxy for urban structures), and radiometric land surface temperature, we develop a machine learning model to predict air temperature, humidity, and heat stress for Chapel Hill, NC. The resulting dataset allows for examination of heat, humidity, and heat stress trends across the entire urban extent, which can aid policymakers in determining key areas to prioritize for heat mitigation measures such as albedo management and shade increase.

Materials and Methods

Study Area

Chapel Hill, NC is a town with a 2021 population of 61,128 (US Census Bureau, 2021) located within the Raleigh-Durham-Cary metropolitan statistical area, spanning the counties of Durham, Orange, and Chatham counties. It is the second largest metropolitan area in the state of North Carolina, with a 2019 population of 2,079,687. Its total area is 21.75 square miles (56.32 km2), with a population density of 2,871.2 people per square mile or 1,107.75 km2 (US Census Bureau, 2021). Chapel Hill is in a humid subtropical climate, according to the Koppen-Geiger climate zone classification (Rubel & Kottek, 2010), with typical temperatures averaging between 32 and 88 degrees Fahrenheit.

Temperature and humidity data collection

Working with local government officials in the Town of Chapel Hill, we identified five areas from the Town of Chapel Hill's Future Land Use Map and Extreme Heat Resiliency Assessment (Town of Chapel Hill, 2020) for citizen scientists to map. These five neighborhoods - 1) Franklin St., 2) Meadowmont; 3) Southern Village; 4) University Place; and 5) Chapel Hill North were areas in Chapel Hill with relatively less tree cover, a higher density of built infrastructure (i.e., buildings, roads) and population (Town of Chapel Hill, 2020). Each were identified as ranking 'high' on the Town's Extreme Heat Vulnerability rating, meaning the town has gauged these areas with the highest number of sensitive populations and highest percentage of developed land cover (>85 percent), with a low amount of tree canopy coverage (<33 percent) (Town of Chapel Hill, 2020). Two to three mile pedestrian routes were determined for each hub to include a variety of land-cover types, from sidewalk, shaded/unshaded, pavement, and grassy. Accessibility considerations were also taken into account to ensure traverse paths were safe for pedestrians and participants could easily and legally walk entire routes. We worked with NOAA to

identify an ideal hot day to conduct the citizen heat mapping campaign, which was identified as Saturday, August 28, 2021. Citizen volunteers were recruited using email lists sent by the Town of Chapel Hill and Museum of Life and Science, as well as from the UNC Chapel Hill community. Since our Institutional Review Board exemption only covered adults over the age of 18, our volunteers had to be over the age of 18 to participate, even though no sensitive or personal data were collected. Participants were sent walking routes prior to the study and were asked to perform a health assessment.

In total around 40 citizen volunteers participated in two mapping sessions: in the afternoon (2-3 pm), and in the early evening (5-6 pm) to capture both daytime and evening temperature and humidity measurements. Since no participants volunteered for Southern Village's evening time period, we only recorded measurements for the afternoon for this neighborhood.

Pocketlab sensors

For data collection, we utilized PocketLab(™) Weather sensors containing a three-in-one BME280 module that embeds sensors to gauge temperature, humidity, and barometric pressure. In our study, we set the PocketLab sensors to collect ambient temperature and relative humidity data every 1 second (Table 1). Participants were asked to place the PocketLab sensors on the palm of their hands so that the temperature and humidity ports, which are located on the sides of the sensor casing, were not obstructed. During our preliminary testing of the devices, we determined that body temperature does not warm the device or lead to an increase in temperature measurement. We asked participants to allow the sensors to acclimate for a few minutes before recording.

Since the ground-level air temperature and humidity data were collected by different volunteers during two separate sessions, we made some adjustments to the data. We removed readings recorded within the first and last two minutes of a participants' mapping assuming that they may have been initializing or finalizing their route. We also removed outliers greater than 3 standard deviations around the mean from our model following Chapman et al., (2017)'s study on UHI using crowdsourcing data. The spatial resolution of the sensors is 10^{-5} degree (approximately 1m). Since some volunteers mapped the same route during the same time of day, we averaged overlapping readings to avoid data duplication.

Spectral and remote sensing data collection

To develop city-wide maps of air temperature, humidity, and heat stress, we collected multi-spectral satellite remote sensing imagery, including land surface temperature, Land use/land cover (LULC). Since UHI intensity is related to LULC (Chen et al., 2006), we combined some of this multi-spectral data to calculate common indices for greenness, Normalized Difference Vegetation Index or NDVI (Chen et al., 2014), and built-up area, Normalized Difference Built Index or NBDI (Zha et al., 2003) (Table 3). We also collected high-resolution aerial imagery from the USGS National Agriculture Imagery Program (Earth Resources Observation And Science (EROS) Center, 2017).

1. Landsat Land Surface Temperature (LST) data

Studies have found positive correlation between satellite-derived Land Surface Temperature (LST) and air temperature (Mildrexler et al., 2011; Zhang et al., 2014) and LST data have been widely used as a proxy for urban heat exposure (T. Chakraborty et al., 2019; Hsu et al., 2021; Manoli et al., 2019; Mentaschi et al., 2022; Zhao et al., 2018). In this study the LST data from satellite sensors Landsat 8 and

MODIS were examined, since both data sources have their advantages and trade-offs. After comparing the spatial and temporal coverage of both sources of data, we decided to use the LST data from Landsat 8 for its higher spatial resolution (30m) and temporal coverage for the time period we sampled. One cloud-free scene closest to the citizen-collected data on August 24, 2021 from Landsat 8 was selected. Based on the National Weather Service, the scene captured date and data collection date have similar daytime temperature ranges, where temperatures range from 19.4°C to 32.8 °C v.s. 22.2 °C to 33.9 °C respectively. To reduce the dependency on a single date LST data and add robustness to the model, averaged LST data for August and September 2021 was also added as an independent variable. We filtered out any scene with 10 percent of cloud coverage or more during this time window.

2. Land use/land cover (LULC)

Studies have found that different LULC types directly result in temperature variance at and near the earth's surface because of different biophysical effects, which include land-surface energy exchanges (Li & Wang, 2019; Mahmood et al., 2013). Since ground temperature data is measured in 2021 and land use/land cover data is from 2020, we assume that patterns in near surface air temperature and its anomalies are consistent temporally.

3. Satellite-derived indices

Although we make the assumption that LULC types have a consistent impact on the near surface air temperature and the anomalies between the years 2020 and 2021, there might be seasonal variance in air temperature and potential LULC change. We incorporate NDVI and NBDI – two commonly-used satellite derived indices that have established relationships with UHI (Chakraborty et al., 2019) to aid in prediction for air temperature and relative humidity. NDVI indicates vegetation coverage or "greenness" and can distinguish between different LULC types and aid in understanding the relationship between vegetation and UHI (Rouse et al., 1974). NDBI, developed by Zha et al., (2003), as well as capture any new urban development of the study area between 2020 and 2021. Both indices are calculated with the satellite image from Sentinel-2 on September 5, 2021 – the latest available and cloud free scene since data collection (Table 3).

4. The National Agriculture Imagery Program (NAIP)

The National Agriculture Imagery Program acquires aerial imagery at 1-m resolution during the "leaf-on" season in the continental U.S starting from 2003. NAIP imagery is available every 2-3 years for each state. This high-resolution multispectral product can provide the details of landcover/landuse, building structure,etc for the urban area. All four bands of NAIP (Red, Green, Blue, Near-infrared), imagery were evaluated as input variables.

Model selection and comparison

We evaluated several machine learning models to predict air temperature, humidity and heat stress across the entire spatial extent of our study area: multilinear regression (MLR), support vector regression (SVR) random forest (RF), and XGBoost. The multilinear regression (MLR) based model is one of the most popular multidimensional interpolation algorithms in UHI studies for its ability to capture the correlation between the UHI and the intra-urban environment variances (Voogt & Oke, 2003). We used MLR as the baseline model to compare the performance of other models because it is easy to implement. Support Vector Regression (SVR) with a radial kernel is an extension of the classifier Support Vector Machine

(SVM). Studies on at or near surface air temperature modeling have found this estimator results in a lower root mean square error (RMSE) compared with other more complex algorithms (Chevalier et al., 2011; Paniagua-Tineo et al., 2011). Random Forest (RF) regression is a nonparametric machine learning algorithm and known for picking up the non-linear relationship between the input variables (Breiman, L., 2001). RF has been applied to multiple studies producing high-resolution land surface temperatures from relatively coarse data and shown solid performance when combining with satellite-derived indices (Hutengs & Vohland, 2016; Y. Yang et al., 2017). XGBoost is one of the state-of-art regression models based on the gradient boosting decision tree model. We used root mean square error (RMSE) and r^2 as the model comparison matrix to evaluate how selected models performed on both training and test dataset.

We implemented the ML algorithms in the R Statistical Computing Environment (version 4.2). MLR is included within R version 4.2; SVM and RF are from R package caret version 6.0-92 (Kuhn, 2008); and XGBoost from XGBoost R package version 1.6.0.1 (T. Chen & Guestrin, 2016). All selected models, except MLR, are controlled by a set of hyperparameters, which constrain the learning process (L. Yang & Shami, 2020). The hyperparameters in SVM are the penalty parameter for the error term, which controls the margin of the decision boundary and sigma, which defines the distance between support vectors and the decision boundary. how far the training data points can be from the decision boundary to be considered. In RF, we tune the model with the number of trees, number of variables randomly sampled as candidates at each split, the minimum number of observations in a terminal node, and the matrix to use to split the data into two branches. In XGBoost, hyperparameters include the maximum depth of the tree, the learning rate, the minimum sum of weight in a node, and minimum loss reduction. We chose root mean square error (RMSE) and r^2 as the model comparison matrix to examine how each model performs on both the training and test datasets. We tuned each model with 5-fold cross validation on a range of parameters to achieve the best parameters resulting in lowest RMSE and highest r^2 on the data's test set.

Two sets of variables were evaluated with all four models. The first set with all variables is described in Table 3, while the second set removed all NAIP bands, since the NAIP data is from 2018 and the vegetation and urban extent information may have changed in the past 3 years. Meanwhile, in the input variables, Sentinel- 2 NDVI and NDBI are providing the similar vegetation and built-up date information and are most up to date. To reduce the model redundancy, we set up the second set variables for comparison. SVM models are sensitive to feature scaling, as SVM takes input variables to find the margins of hyperplanes to best separate the data. The distances between data points with and without scaling are different. Thus, the SVM can be biased if trained with un-scaled data. To improve the performance of SVM models, we scaled and centered the continuous variables with a preprocessing function (*prePrecoss*) from R package caret version 6.0-92. These two preprocess methods subtracts the mean of the input variables from them to have a mean of zero for each variable and divide each variable by its standard deviation such that each variable has a standard deviation of 1.

Model evaluation and final selection

Supplementary Table S1and S2 shows the results of air temperature prediction from each model with the best parameters. The RF and XGBoost model have similar test RMSE and r2 for both sessions, but outperform the other two models by resulting in lower test RMSE (for session 1: - 1.1 °C on RF v.s MLR; -1.3 °C on XGBoost v.s MLR; - 0.16 °C on RF v.s SVM; - 0.18 °C on XGBoost vs. SVR) and higher r2. For the computation time, RF model training is about 7 times faster than XGBoost training on a

8 cores windows PC. Comparing the results from different sets of variables with the same model, the set without NAIP has better results in both sessions (Table S2). Based on the results from both sets of variables with all four selected models, we decided to use the RF model and the dataset without NAIP for its good overall prediction performance and fast computation on our dataset. The best performed air temperature model results in a RMSE = 0.76 °C, r^2 = 0.86 on the test data for the afternoon (2-3 pm) session and RMSE = 0.48 °C, r^2 = 0.91on test data for the evening (5-6 pm). We used the same input variables as air temperature model and RF as estimators to build the relative humidity models. The best performing humidity model results in a RMSE = 1.50%, r^2 = 0.91 on the test dataset for afternoon session 2-3 pm and RMSE = 1.32% , r^2 = 0.89 on the test dataset for the evening session 5-6 pm.

To better understand the key predictors for air temperature and humidity, we ran Monte Carlo cross-validation (T. C. Chakraborty et al., 2021; Xu & Liang, 2001) 50 times with random training and validation splits and evaluated the input features with permutation feature importance scores.

Heat stress calculation - Humidex

To get an estimate of the human physiological response to heat, we use the humidex, an operational metric of moist heat stress (Masterton & Richardson, 1979). Humidex is calculated for each pixel using the estimates of air temperature (T) and relative humidity (RH) from the RF models. First, we calculate dew point temperature (T_d) from the following equation:

$$T_d = \frac{243.04 \times \left\{ ln\left(\frac{RH}{100}\right) + \frac{17.625 \times T}{243.04 + T} \right\}}{17.625 - \left\{ ln\left(\frac{RH}{100}\right) + \frac{17.625 \times T}{243.04 + T} \right\}} \quad (1)$$

Then humidex is computed from:

$$Humidex = T \ + 0.5555 \times \left(6.11 \times e^{5417.753 \times \left(\frac{1}{273.16} - \frac{1}{273.15 + T_d}\right)} - 10 \right) \quad (3)$$

Note that humidex is a unitless proxy for how hot it feels under shade, and results should be interpreted keeping this caveat in mind.

Air temperature, humidity, and Humidex prediction

After model evaluation, we re-trained the model with all of the citizen science data to generate the final model. We then used the final model with independent variables that cover the whole study area at 10 meter spatial resolution as inputs to predict the air temperature and relative humidity. We also used the predicted air temperature and relative humidity to calculate the humidex as a proxy to simulate pedestrians' thermal comfort under shade. Finally, the predicted air temperature, relative humidity, and Humidex results were converted into gridded raster layers with the *rasterio(version 1.0.21)* package in Python.

Sociodemographic analysis

To explore disparities by sociodemographic group in Chapel Hill, replicating similar analyses in previous studies (Benz & Burney, 2021; T. Chakraborty et al., 2019; Hsu et al., 2021) that used primarily LST, we extracted census tract and block group demographic data for Chapel Hill from the 2020 ACS 5-year Data

Profile (US Census Bureau, 2020). Since some areas of Chapel Hill's jurisdictional limits cover census tracts in other counties, we included additional census tracts in this analysis that overlap, which explains why our urban extent slightly differs from Chapel Hill's own administrative boundaries (Supplementary Figure S1). Median household income and race, according to the U.S. Census's categorizations of White, Black, Asian, Pacific Islander, Native American, and Other were extracted. For examining racial disparities, we use census tracts, the smallest level of aggregation for which the race data are available. To examine income-based disparities, we use census block groups.

The observed LST and predicted air temperature, humidity, and Humidex are aggregated to the census tracts and block groups. Associations between income and the heat exposure metrics are examined using Pearson's correlations in R language. Sensitivities of these metrics to increases in income can be represented by the correlation coefficients or the slopes of the lines of best fit between the two variables. To examine race-based disparity, we calculated population-weighted heat exposures for each census group, following the method in Hsu et al. (2021).

Results

Individual-scale air temperature and humidity

Although weather forecasts showed a predicted high temperature of 35°C and low temperature of 22°C for August 28, 2021, our citizen volunteers mapped much higher air temperatures in all five hubs, ranging from 33.3°C to 42.6°C in the afternoon session, and 29.9°C to 39.2°C in the evening session (Figure S3; Figure 1). The highest temperatures were measured during the early afternoon session in the Franklin St. (38.7 ± 2.0 °C) and University Place (39.1 ± 1.4 °C) neighborhoods, which feature a high proportion of asphalt parking lots and pavement, compared to surrounding areas and other hubs (Figure 1).

Volunteer-collected relative humidity ranged from 30% to 58.9% in the afternoon session and 33.8% - 58.2% for the evening session. Although the relative humidity ranges are similar between the two time periods, we still observed differences in the humidity distribution between hubs. Franklin St. (38.6 ± 3.4 %) and University Place (38.5 ± 4.4 %) are the driest neighborhoods. The Meadowmont neighborhood, located in the southeast area of Chapel Hill, has relatively high humidity in both time periods (48.7 ± 2.3% for the afternoon; and 44.2 ± 2.3% in the evening), which may be related to high vegetation and tree coverage in the neighborhood. Chapel Hill North showed the largest differences in humidity between the afternoon (39.37± 3.23%) and evening (47.25± 6.09%) sessions. One explanation for this disparity may be due to variations in the mapping routes for this neighborhood between the two time periods, where volunteers mapped the built-up and parking lots during the afternoon session, while they mapped more residential areas with high tree coverage during the evening session (See Figure S3, c and d).

Predictors of air temperature and relative humidity

Figure 2 shows the importance scores of all features in the air temperature and relative humidity models for the afternoon (2-3pm) session. Based on the permutation feature importance, which indicates how much the model depends on each input feature determined by how much the model score decreases when a certain feature is removed, the Landsat 8 two-month averaged LST is the top ranking predictor for both

the air temperature and relative humidity models. The next most important features include the Landsat 8 LST data closest to the citizen-science data collection date. NDVI and NDBI also have high contributions to both the air temperature and humidity models. Among all five land cover/ land use dummy variables, whether an area is classified as the 'tree' land cover class has the most predictive effect in the air temperature and humidity models.

Since relative humidity is inversely correlated with air temperature (Chakraborty et al., 2022), we also found an inverse relationship with input features with air temperature vs. relative humidity from our citizen science data (Figures S4 and S5).

Modeled air temperature, humidity, and Humidex

Figure 3 shows predicted air temperature, relative humidity, and humidex for the afternoon and evening in our study area. Overall, we found the afternoon is hotter and drier than the evening, with the predicted mean air temperature as 35.9±0.7°C for afternoon session and 32.3±1.9°C for evening session; the predicted mean relative humidity as 40.7±1% for afternoon session and 56.3±1% for evening session. Also we found different patterns of the heat distribution between the afternoon session and evening sessions. The afternoon session tends to be more uniformly hot over the study area, where 90% of the area's predicted air temperature ranges from 35.1°C (5th percentile) to 37.4 °C (95th percentile) and has a standard deviation of 0.7°C. In the evening session, the predicted air temperature varies more across the study area, with 90% of the area ranging from 30.5°C (5th percentile) to 35.5°C (95th percentile) with a 1.9 °C standard deviation. As a function of air temperature and relative humidity, the Humidex shows similar patterns as predicted air temperature and relative humidity on both sessions. In the afternoon session, the Humidex ranges from 42.3 (5th percentile) to 46.6 (95th percentile) for 90% of the study area, with an average value of 44±1.3. In the evening session, the Humidex varies from 38.4 (5th percentile) to 48.7 (95th percentile) for 90% of the study area, with values on average 42.3±3.8.

Land cover analysis

Based on the ESA Worldcover 2020 data, our study area has seven land cover types: 82.8% of the total area is classified as Trees, followed by 9.8% Built-up area and 6.2% Grassland. The remaining 1.2% of the area is classified as Barren or sparse vegetation, Open water, Cropland, and Herbaceous wetland (See Figure 4b and Table 4). In Table 4, we determined predicted afternoon air temperature by land cover classes, and calculated each land cover class's temperature difference from the Tree cover class, since it has the coolest predicted air temperature compared to other land cover classes. On average the Built-up area is 1.2°C hotter than tree-covered areas and Grassland is 0.7 °C hotter. Our study area also contains a small open water body and the predicted air temperature of the water body is 0.3°C cooler than the tree-covered area. Figure 6a shows the mean air temperature differences from the tree class. Half of the study area is hotter than mean air temperature of the Tree class, with 31.5% of the total area 0-1°C hotter; 13.3% area 1-2 °C hotter; and only 2% area 2°C hotter.

Sociodemographic Analysis by Census Tracts

While some obvious spatial patterns in heat, greenness, race, and income can be observed by census tract (Figure 5), we did not find substantial differences in the exposure heat metrics between these different racial demographic groups (Supplementary Table 3), except a minor difference in LST between White and Black (33.2°C versus 33.2°C). The hottest census tracts (in Figure 5, those with the highest average

Humidex) are found in the downtown area of Chapel Hill (tracts 116.01 and 116.02), which also has the lowest NDVI (a proxy for tree cover and greenness). These census tracts correspond with the University of Chapel Hill and Franklin Street neighborhood, which has a high student population and explains why these areas have the lowest income per capita (Krizek, 1995). According to the 2020 ACS Census, 76 percent of Chapel Hill residents identify as White, 13 percent as Asian, 10 percent as Black, and less than 2 percent as Native American or Other. Populations living within census tracts are predominantly White (76±11 percent), followed by Asian (12.6±8.6) and Black (9.4±7.2 percent) (see Figure S6).

Socioeconomic analysis of income by census block group

All three heat metrics (LST, predicted air temperature, and humidex) show inverse relationships with income, meaning as income increases, temperature and humidex decrease. The sensitivities of the various heat metrics to changes in income, however, are different. As income increases by $10,000, LST drops by 0.34 °C, but air temperature drops by only 0.05 °C and Humidex drops by .1 (Figure 6).

Discussion

This study provides a replicable method for modeling spatially-resolved air temperature, humidity, and heat stress over an urban area and engages citizens to gather air temperature and humidity data, which are used to train the models. Since high-resolution, individual-scale air temperature, humidity and heat stress data are difficult and costly to monitor, this study sought to develop an approach using low-cost, consumer-grade sensors combined with satellite remote sensing data and machine learning to map urban heat over various land-cover classes to understand intra-urban spatial variability of heat at a relatively high resolution (10 meters). To the authors' knowledge, this study is also one of the first to use machine learning methods to predict relative humidity, which allowed for prediction of a common heat stress metric (Humidex) across an urban area. While previous studies have argued against the use of satellite-derived LST as a proxy for air temperature and heat stress (Chakraborty et al., 2022; Turner et al., 2022), we find that, when combined with other ancillary information, satellite-derived LST can be a strong predictor of air temperature. Since our machine learning model identified both the Landsat 2-month and the closest time period as being the variables contributing the most predictive power to our model, air temperature variability is embedded within LST variability, which is reflected in our machine learning algorithm. The strength of correlations between LST and air temperature is not 1, which is important for studying disparities in heat exposure and we discuss further below. For instance, we find that LST is more sensitive to income than air temperature (Figure 6), which Chakraborty et al. (Under Review) also observed across other U.S. cities. The resulting datasets and maps can be utilized within various decision making contexts, from individuals determining where to live or urban planners and policymakers developing urban heat mitigation measures to protect citizens. We discuss some of our key findings and their implications for policy below as well as some of the study's limitations.

Individual heat exposure and stress

Our findings here show that individuals may be exposed to higher levels of heat and heat stress than what weather station data provide, and this heat varies according to land cover type and throughout the day. With our volunteer-collected data, we found air temperatures ranged from 33.3°C to 42.6°C - on average 10°C higher than what weather forecasts showed for the day of data collection. We observed multiple instances of temperature readings higher than 40 degrees C or 104 degrees F, which the National Weather

Service (NWS) classifies as 'extreme caution' (32-41°C), and several readings that fall into the NWS's 'danger' zone (41-54°C). The hottest areas, Franklin St. (38.7°C±2.02 during the afternoon) and University Place (39.1°C±1.4 during the afternoon), tended to intersect with census tracts that had the lowest greenness or NDVI (mean 0.54 for Franklin Street and 0.46 for University Place, compared to 0.61 for Southern Village) and the least amount of classified tree land cover class (less than 0.5 for Franklin Street and 0.65 for University Place, compared to 0.88 for Chapel Hill North and 0.85 for Southern Village). The Franklin Street area is also located within census tracts that have the highest average built-up area (average 0.51, compared to 0.09 in Chapel Hill North). The Franklin Street area corresponds with the census tracts with the highest average humidex values out of all hubs (Figure 5), likely due to its relative lack of tree cover and greater built extent compared to other areas of Chapel Hill.

While temperatures tended to cool off to the 29.9°C to 39.2°C range in the evening, some of the hubs, such as the Meadowmont neighborhood, showed much less variation between the early afternoon and evening temperatures, with a difference in median temperature only 0.1°C, compared to other neighborhoods, such as Franklin Street (4.3°C) and University Place (4.4°C). This much smaller difference between daytime and evening UHI is concerning from a public health perspective, given prior research demonstrating prolonged exposure to high nighttime temperatures increases the probability of mortality in extreme heat conditions (Laaidi et al., 2012).

Sensitivity to income

Although we did not find substantial variation in air temperature, humidity or heat stress by racial demographic, since the majority of census tracts in Chapel Hill are predominantly white (Figure S6), we determined that income is negatively associated with our heat metrics, albeit with varying sensitivities. We observed the greatest sensitivity in LST, where $10,000 greater income results in a drop in average temperature of 0.34°C, although this sensitivity was much less for our predicted air temperature (0.05°C) and humidex (0.1). These results are consistent with greater intra-urban variability seen for LST compared to air temperature and moist heat stress from observational studies (Chakraborty et al., 2022; Ho et al., 2016; Turner et al., 2022) and higher magnitude of disparities for LST than for air temperature and humidex over US cities from numerical weather model simulations (Chakraborty et al., 2022). The differences in income sensitivity for various heat metrics illustrates the need for decisionmakers to be cautious when applying these findings for policy decisions, since different conclusions can be drawn based on which heat metric is selected. In our analysis, the lowest income areas also correspond to census tracts with a significant proportion of the population between ages 20-24: the Franklin Street census tracts have more than 43 percent of the population in this demographic, compared to census tracts in the Chapel Hill North neighborhood, with only around 5 percent of the population in this age bracket (Figure 5). Since the University of North Carolina at Chapel Hill surrounds the Franklin Street neighborhood, the high percentage of people aged 20-24 living in these census tracts makes sense and explains the relatively lower income compared to neighboring census tracts.

While relative humidity shows an inverse relationship with air temperature (Figure S5), which is expected within urban areas due to urbanization-induced drying (Chakraborty et al. 2022), the overall sensitivity of humidex to income is higher than that for air temperature (Figure 6). This is an interesting result that requires further clarification. Humidex is an unitless metric of heat stress and is not expressed in °C, and should ideally not be compared to our other heat metrics of air temperature and LST. Moreover, Humidex

has a much higher baseline and range of values than air or surface temperature, which would influence these sensitivities within a linear model as used in Figure 6. Finally, a unit change in Humidex is not equivalent to a unit °C change in air temperature from a human health context. As such, it is important to link these variabilities to actual health outcomes to better contextualize the importance of these numerical values. The relative importance of humidity for human heat risk is still an active area of research (Sherwood, 2018) and different metrics of moist heat stress would have different sensitivities to income, although all are expected to be weaker than the sensitivity to LST (Chakraborty et al. 2022). Finally, heat stress also depends on wind speed, solar radiation, etc., which can be modified by urban morphology, shading structures, etc. These factors should be considered in future studies to better understand the heterogeneity of heat stress within urban environments.

Policy implications for mitigating and managing urban heat

The resulting air temperature, humidity, and heat stress maps and datasets can be used to inform urban heat mitigation planning and policy. Identification of urban heat hotspots, combined with sociodemographic data, can help identify potential vulnerable communities and areas for targeted intervention. Our findings that tree-covered areas, aside from water bodies, are the coolest, with built-up urban areas and grasslands (e.g., parks or unshaded greenspaces) 1.2°C and 0.7°C warmer, respectively, is in line with previous studies (Zhao et al., 2014; Aboelata et al., 2020; Shah et al., 2021; Aram et al., 2019; Ziter et al., 2019) that suggest albedo management, through tree planting or green space development, could help mitigate the UHI. Since the hottest areas of Chapel Hill are coincident with the highest population density, lowest greenness, and lowest income, policymakers could use the data and maps we produced here to develop strategies to increase green space, tree cover, and shade in particularly hot areas. Cities are starting to incorporate insights derived from high-resolution heat mapping into urban planning decisions. For example, in the case of Raleigh, NC, data collected from a July 2021 NOAA heat mapping campaign led to a city council vote to reallocate $70,000 into a pavement rejuvenation project to coat more than 150,000 yards with titanium dioxide to make it more reflective (Retana, 2022).

Limitations

Our method is certainly not immune from limitations. First, the PocketLab sensors themselves have their own sources of error. For example, the sensor has a 3 percent absolute accuracy for measuring relative humidity, which means the measured relative humidity can deviate from the true value by 3 percent. Similarly, the sensor has an absolute accuracy for temperature measurements of 0.5 degrees Celsius. These ranges of absolute accuracy could certainly affect the accuracy of our predictions for the entire urban extent. Second, volunteers pose another source of error, since most of them were first-time users of the PocketLab sensors. Although we provided the volunteers training before collecting measurements, there could be some individual error introduced. For instance, when evaluating the quality of data collected, we found one user's recorded humidity data was extremely low while air temperature data appeared within a normal range. This error may be due to a temporary issue with the sensor or an individual's accidental blockage of the humidity sensor port. One way to evaluate the sensitivity of our data to these possible errors, future studies could expand data collection involving more volunteers and a larger study area.

Conclusion

This study has developed a method for applying satellite remote sensing and citizen-collected air and humidity data to develop a high resolution (10 meter) map of air temperature, humidity, and heat stress. We confirm previous studies that show air temperatures are hottest over impervious, built-up urban areas and coolest over forested, tree-covered areas. Compared to singular weather station measurements, we find individuals are exposed to much higher air temperatures and heat stress, and that this exposure is greatest during the daytime and cools off in the evening, although the amount of this difference between daytime and nighttime differs. We further establish a negative relationship between income and heat, although the sensitivity of this relationship varies based on the heat metric, with satellite-based land surface temperature showing the greatest sensitivity to income. Ultimately, this method and approach can be replicated and scaled at a relatively low cost and provide much more detailed information for decisionmakers and urban planners seeking to mitigate urban heat and its human health effects.

Acknowledgements
We are grateful for the 40 volunteers who participated in this study and assisted us to collect the air temperature and humidity measurements. This study was supported by the Samuel Family Foundation (Grant No: 5116545). We thank John Richardson, Chief Resilience Officer of the Town of Chapel Hill and the Town of Chapel Hill for allowing us to conduct this study and set up hubs in public spaces to coordinate volunteers. We thank Max Cawley, Senior Community Manager, Museum of Life and Science, Dana Haine of UNC's Institute for Environment, for providing PocketLab sensors for data collection. We thank Ian French (Yale-NUS College '22) and Joyce Mei (Cornell University '24) for their assistance in testing the PocketLab sensors and planning the walking routes. We thank members of the Data-Driven EnviroLab team for coordinating the neighborhood hubs - Katherine Burley, Brendan Mapes, Marco Schletz, and Varun Subramanian. We also thank Myleigh Neill from the State Climate Office of North Carolina for providing support on the day of data collection.

Ethical Statement
Data collection by citizen volunteers was reviewed and exempted by UNC's Institutional Review Board Committee (Project ID: 21-1748).

References
Benz, S. A., & Burney, J. A. (2021). Widespread Race and Class Disparities in Surface Urban Heat Extremes Across the United States. *Earth's Future*, *9*(7), e2021EF002016. https://doi.org/10.1029/2021EF002016

Breiman, L. (2001). Random Forests. *Machine Learning*, *45*, 5–32.

Chakraborty, T. C., Newman, A., Qian, Y., Hsu, A., & Sheriff, G. (2022). *Residential Segregation and Urban Heat Stress Disparities in the United States* (SSRN Scholarly Paper No. 4231649). https://doi.org/10.2139/ssrn.4231649

Chakraborty, T. C., Sarangi, C., & Lee, X. (2021). Reduction in human activity can enhance the urban

heat island: Insights from the COVID-19 lockdown. *Environmental Research Letters*, *16*(5), 054060. https://doi.org/10.1088/1748-9326/abef8e

Chakraborty, T., Hsu, A., Manya, D., & Sheriff, G. (2019). Disproportionately higher exposure to urban heat in lower-income neighborhoods: A multi-city perspective. *Environmental Research Letters*, *14*(10), 105003.

Chakraborty, T., Hsu, A., Manya, D., & Sheriff, G. (2020). A spatially explicit surface urban heat island database for the United States: Characterization, uncertainties, and possible applications. *ISPRS Journal of Photogrammetry and Remote Sensing*, *168*, 74–88.

Chakraborty, T., Venter, Z. S., Qian, Y., & Lee, X. (2022). Lower urban humidity moderates outdoor heat stress. *AGU Advances*, *3*(5), e2022AV000729.

Chapman, L., Bell, C., & Bell, S. (2017). Can the crowdsourcing data paradigm take atmospheric science to a new level? A case study of the urban heat island of London quantified using Netatmo weather stations. *International Journal of Climatology*, *37*(9), 3597–3605.

Chen, T., De Jeu, R. A. M., Liu, Y. Y., Van der Werf, G. R., & Dolman, A. J. (2014). Using satellite based soil moisture to quantify the water driven variability in NDVI: A case study over mainland Australia. *Remote Sensing of Environment*, *140*, 330–338.

Chen, T., & Guestrin, C. (2016). XGBoost: A Scalable Tree Boosting System. *Proceedings of the 22nd ACM SIGKDD International Conference on Knowledge Discovery and Data Mining*, 785–794. https://doi.org/10.1145/2939672.2939785

Chen, X.-L., Zhao, H.-M., Li, P.-X., & Yin, Z.-Y. (2006). Remote sensing image-based analysis of the relationship between urban heat island and land use/cover changes. *Remote Sensing of Environment*, *104*(2), 133–146. https://doi.org/10.1016/j.rse.2005.11.016

Chevalier, R. F., Hoogenboom, G., McClendon, R. W., & Paz, J. A. (2011). Support vector regression with reduced training sets for air temperature prediction: A comparison with artificial neural networks. *Neural Computing and Applications*, *20*(1), 151–159. https://doi.org/10.1007/s00521-010-0363-y

Earth Resources Observation And Science (EROS) Center. (2017). *National Agriculture Imagery Program (NAIP)* [Tiff]. U.S. Geological Survey. https://doi.org/10.5066/F7QN651G

Heal, G., & Park, J. (2016). Reflections—temperature stress and the direct impact of climate change: A review of an emerging literature. *Review of Environmental Economics and Policy*.

Ho, H. C., Knudby, A., Sirovyak, P., Xu, Y., Hodul, M., & Henderson, S. B. (2014). Mapping maximum urban air temperature on hot summer days. *Remote Sensing of Environment*, *154*, 38–45.

Ho, H. C., Knudby, A., Xu, Y., Hodul, M., & Aminipouri, M. (2016). A comparison of urban heat islands mapped using skin temperature, air temperature, and apparent temperature (Humidex), for the greater Vancouver area. *Science of the Total Environment*, *544*, 929–938.

Hoffman, J. S., Shandas, V., & Pendleton, N. (2020). The Effects of Historical Housing Policies on Resident Exposure to Intra-Urban Heat: A Study of 108 US Urban Areas. *Climate*, *8*(1), Article 1. https://doi.org/10.3390/cli8010012

Hsu, A., Sheriff, G., Chakraborty, T., & Manya, D. (2021). Disproportionate exposure to urban heat island intensity across major US cities. *Nature Communications*, *12*(1), 1–11.

Huang, K., Lee, X., Stone Jr, B., Knievel, J., Bell, M. L., & Seto, K. C. (2021). Persistent increases in nighttime heat stress from urban expansion despite heat island mitigation. *Journal of Geophysical Research: Atmospheres*, *126*(4), e2020JD033831.

Hutengs, C., & Vohland, M. (2016). Downscaling land surface temperatures at regional scales with random forest regression. *Remote Sensing of Environment*, *178*, 127–141. https://doi.org/10.1016/j.rse.2016.03.006

IPCC. (2021). Summary for Policymakers. In *Climate Change 2021: The Physical Science Basis. Contribution of Working Group I to the Sixth Assessment Report of the Intergovernmental Panel on Climate Change* (pp. 3–32). Cambridge University Press. https://doi.org/10.1017/9781009157896.001

Krayenhoff, E. S., Moustaoui, M., Broadbent, A. M., Gupta, V., & Georgescu, M. (2018). Diurnal interaction between urban expansion, climate change and adaptation in US cities. *Nature Climate*

Change, *8*(12), Article 12. https://doi.org/10.1038/s41558-018-0320-9

Krizek, K. J. (1995). Patterns of use in Main Street activity: A case study of downtown Chapel Hill, NC. *Carolina Planning*, *20*(2), 62–70.

Kuhn, M. (2008). Building predictive models in R using the caret package. *Journal of Statistical Software*, *28*, 1–26.

Laaidi, K., Zeghnoun, A., Dousset, B., Bretin, P., Vandentorren, S., Giraudet, E., & Beaudeau, P. (2012). The impact of heat islands on mortality in Paris during the August 2003 heat wave. *Environmental Health Perspectives*, *120*(2), 254–259.

Li, D., & Wang, L. (2019). Sensitivity of Surface Temperature to Land Use and Land Cover Change-Induced Biophysical Changes: The Scale Issue. *Geophysical Research Letters*, *46*(16), 9678–9689. https://doi.org/10.1029/2019GL084861

Mahmood, R., Keeling, T., Foster, S. A., & Hubbard, K. G. (2013). Did irrigation impact 20th century air temperature in the High Plains aquifer region? *Applied Geography*, *38*, 11–21.

Manoli, G., Fatichi, S., Bou-Zeid, E., & Katul, G. G. (2020). Seasonal hysteresis of surface urban heat islands. *Proceedings of the National Academy of Sciences*, *117*(13), 7082–7089.

Manoli, G., Fatichi, S., Schläpfer, M., Yu, K., Crowther, T. W., Meili, N., Burlando, P., Katul, G. G., & Bou-Zeid, E. (2019). Magnitude of urban heat islands largely explained by climate and population. *Nature*, *573*(7772), 55–60.

Martilli, A., Roth, M., & Chow, W. T. (2020). Summer average urban-rural surface temperature differences do not indicate the need for urban heat reduction. *Research Collection School of Social Sciences*, 1–13. https://doi.org/10.31219/osf.io/8gnbf

Masterton, J. M., & Richardson, F. A. (1979). *Humidex: A method of quantifying human discomfort due to excessive heat and humidity*. Environment Canada, Atmospheric Environment.

Mentaschi, L., Duveiller, G., Zulian, G., Corbane, C., Pesaresi, M., Maes, J., Stocchino, A., & Feyen, L. (2022). Global long-term mapping of surface temperature shows intensified intra-city urban heat island extremes. *Global Environmental Change*, *72*, 102441.

Mildrexler, D. J., Zhao, M., & Running, S. W. (2011). A global comparison between station air temperatures and MODIS land surface temperatures reveals the cooling role of forests. *Journal of Geophysical Research: Biogeosciences*, *116*(G3). https://doi.org/10.1029/2010JG001486

Muller, C. L., Chapman, L., Grimmond, C. S. B., Young, D. T., & Cai, X. (2013). Sensors and the city: A review of urban meteorological networks. *International Journal of Climatology*, *33*(7), 1585–1600.

NOAA. (n.d.). *Mapping Campaigns*. National Integrated Heat Health Information System. Retrieved December 6, 2022, from https://www.heat.gov/pages/mapping-campaigns

Oke, T. R. (1982). The energetic basis of the urban heat island. *Quarterly Journal of the Royal Meteorological Society*, *108*(455), 1–24. https://doi.org/10.1002/qj.49710845502

Paniagua-Tineo, A., Salcedo-Sanz, S., Casanova-Mateo, C., Ortiz-García, E. G., Cony, M. A., & Hernández-Martín, E. (2011). Prediction of daily maximum temperature using a support vector regression algorithm. *Renewable Energy*, *36*(11), 3054–3060. https://doi.org/10.1016/j.renene.2011.03.030

Park, R. J., Goodman, J., Hurwitz, M., & Smith, J. (2020). Heat and learning. *American Economic Journal: Economic Policy*, *12*(2), 306–339.

QuickStats: Percentage Distribution of Heat-Related Deaths, by Age Group — National Vital Statistics System, United States, 2018–2020. (2022). *MMWR. Morbidity and Mortality Weekly Report*, *71*. https://doi.org/10.15585/mmwr.mm7124a6

Rajagopalan, P., Andamon, M. M., & Paolini, R. (2020). Investigating thermal comfort and energy impact through microclimate monitoring-a citizen science approach. *Energy and Buildings*, *229*, 110526.

Retana, J. (2022, June 22). Are Raleigh's roads making the city hotter? *CBS17.Com*. https://www.cbs17.com/news/local-news/wake-county-news/are-raleighs-roads-making-the-city-hotter/

Ritchie, H., & Roser, M. (2018). Urbanization. *Our World in Data*.

https://ourworldindata.org/urbanization

Rouse, J. W., Jr., Haas, R. H., Schell, J. A, & Deering, D. W. (1974). Monitoring vegetation systems in the Great Plains with ERTS. *NASA. Goddard Space Flight Center 3d ERTS-1 Symp*, *1*.

Rubel, F., & Kottek, M. (2010). Observed and projected climate shifts 1901-2100 depicted by world maps of the Köppen-Geiger climate classification. *Meteorologische Zeitschrift*, *19*(2), 135.

Shandas, V., Voelkel, J., Williams, J., & Hoffman, J. (2019). Integrating Satellite and Ground Measurements for Predicting Locations of Extreme Urban Heat. *Climate*, *7*(1), Article 1. https://doi.org/10.3390/cli7010005

Sherwood, S. C. (2018). How important is humidity in heat stress? *Journal of Geophysical Research: Atmospheres*, *123*(21), 11–808.

Shi, H., Xian, G., Auch, R., Gallo, K., & Zhou, Q. (2021). Urban Heat Island and Its Regional Impacts Using Remotely Sensed Thermal Data—A Review of Recent Developments and Methodology. *Land*, *10*(8), Article 8. https://doi.org/10.3390/land10080867

Steeneveld, G. J., Koopmans, S., Heusinkveld, B. G., van Hove, L. W. A., & Holtslag, A. a. M. (2011). Quantifying urban heat island effects and human comfort for cities of variable size and urban morphology in the Netherlands. *Journal of Geophysical Research: Atmospheres*, *116*(D20). https://doi.org/10.1029/2011JD015988

Tan, J., Zheng, Y., Tang, X., Guo, C., Li, L., Song, G., Zhen, X., Yuan, D., Kalkstein, A. J., Li, F., & Chen, H. (2010). The urban heat island and its impact on heat waves and human health in Shanghai. *International Journal of Biometeorology*, *54*(1), 75–84. https://doi.org/10.1007/s00484-009-0256-x

Town of Chapel Hill. (2020, December 9). *Future Land Use Map—Update to Chapel Hill 2020*. FlippingBook. https://online.flippingbook.com/view/26191/72-73/?sharedOn=

Turner, V. K., Rogers, M. L., Zhang, Y., Middel, A., Schneider, F. A., Ocón, J. P., Seeley, M., & Dialesandro, J. (2022). More than surface temperature: Mitigating thermal exposure in hyper-local land system. *Journal of Land Use Science*, *17*(1), 79–99.

https://doi.org/10.1080/1747423X.2021.2015003

US Census Bureau. (2020). *American Community Survey 5-Year Data (2009-2020)*. Census.Gov. https://www.census.gov/data/developers/data-sets/acs-5year.html

US Census Bureau. (2021). *U.S. Census Bureau QuickFacts: Chapel Hill town, North Carolina*. https://www.census.gov/quickfacts/fact/table/chapelhilltownnorthcarolina/PST045221

van Hove, L. W. A., Jacobs, C. M. J., Heusinkveld, B. G., Elbers, J. A., van Driel, B. L., & Holtslag, A. A. M. (2015). Temporal and spatial variability of urban heat island and thermal comfort within the Rotterdam agglomeration. *Building and Environment*, *83*, 91–103. https://doi.org/10.1016/j.buildenv.2014.08.029

Vargas Zeppetello, L. R., Raftery, A. E., & Battisti, D. S. (2022). Probabilistic projections of increased heat stress driven by climate change. *Communications Earth & Environment*, *3*(1), 1–7.

Venter, Z. S., Brousse, O., Esau, I., & Meier, F. (2020). Hyperlocal mapping of urban air temperature using remote sensing and crowdsourced weather data. *Remote Sensing of Environment*, *242*, 111791.

Voogt, J. A., & Oke, T. R. (2003). Thermal remote sensing of urban climates. *Remote Sensing of Environment*, *86*(3), 370–384. https://doi.org/10.1016/S0034-4257(03)00079-8

Xu, Q.-S., & Liang, Y.-Z. (2001). Monte Carlo cross validation. *Chemometrics and Intelligent Laboratory Systems*, *56*(1), 1–11. https://doi.org/10.1016/S0169-7439(00)00122-2

Yang, L., & Shami, A. (2020). *On Hyperparameter Optimization of Machine Learning Algorithms: Theory and Practice*. https://doi.org/10.1016/j.neucom.2020.07.061

Yang, Y., Cao, C., Pan, X., Li, X., & Zhu, X. (2017). Downscaling Land Surface Temperature in an Arid Area by Using Multiple Remote Sensing Indices with Random Forest Regression. *Remote Sensing*, *9*(8), Article 8. https://doi.org/10.3390/rs9080789

Zander, K. K., Botzen, W. J., Oppermann, E., Kjellstrom, T., & Garnett, S. T. (2015). Heat stress causes substantial labour productivity loss in Australia. *Nature Climate Change*, *5*(7), 647–651.

Zha, Y., Gao, J., & Ni, S. (2003). Use of normalized difference built-up index in automatically mapping

urban areas from TM imagery. *International Journal of Remote Sensing*, *24*(3), 583–594. https://doi.org/10.1080/01431160304987

Zhang, P., Bounoua, L., Imhoff, M. L., Wolfe, R. E., & Thome, K. (2014). Comparison of MODIS Land Surface Temperature and Air Temperature over the Continental USA Meteorological Stations. *Canadian Journal of Remote Sensing*, *40*(2), 110–122. https://doi.org/10.1080/07038992.2014.935934

Zhao, L., Lee, X., Smith, R. B., & Oleson, K. (2014). Strong contributions of local background climate to urban heat islands. *Nature*, *511*(7508), Article 7508. https://doi.org/10.1038/nature13462

Zhao, L., Oppenheimer, M., Zhu, Q., Baldwin, J. W., Ebi, K. L., Bou-Zeid, E., Guan, K., & Liu, X. (2018). Interactions between urban heat islands and heat waves. *Environmental Research Letters*, *13*(3), 034003.

Ziter, C. D., Pedersen, E. J., Kucharik, C. J., & Turner, M. G. (2019). Scale-dependent interactions between tree canopy cover and impervious surfaces reduce daytime urban heat during summer. *Proceedings of the National Academy of Sciences*, *116*(15), 7575–7580. https://doi.org/10.1073/pnas.1817561116

Zumwald, M., Knüsel, B., Bresch, D. N., & Knutti, R. (2021). Mapping urban temperature using crowd-sensing data and machine learning. *Urban Climate*, *35*, 100739.

Table 1. PocketLab sensor specifications

	Humidity	Temperature
Range	0-100 %RH	-40 - 85 C (-40 - 185 F)
Resolution	0.02 %RH	0.01 C (0.02 F)
Absolute Accuracy	3 %RH	0.5 C (0.9 F)

Table 2. Descriptive statistics of temperature and relative humidity data collected by citizens.

Session	No. of volunteers	Variable	Count	Min	Mean	Median	Max	St.Dev.
2-3 pm	13	Temperature(° C)	20551	33.34	37.76	37.69	42.59	2.00
2-3 pm	13	Relative Humidity (%)	20471	30.02	40.36	39.49	58.93	5.04
5-6 pm	15	Temperature(° C)	12996	29.86	34.69	35.05	39.22	1.59
5-6 pm	15	Relative Humidity(%)	12552	33.82	45.24	45.04	58.22	3.96

Table 3. Overview of spectral data collected.

Date Type	Spatial Resolution	Temporal Resolution	Data Source	Data Acquired Time	Data Layer Calculation
Land Surface Temperature	30m	16 days	Landsat 8	August 24, 2021; Average LST of August and September, 2021	-
Land use/land cover (LULC)	10m	-	ESA Worldcover 2020	2020	-
Satellite-derived Indices	10-20m	8 days	Sentinel-2	Average of images on September 5 and 10, 2021	NDVI = (NIR - Red)/(NIR + Red) NDBI = (SWIR - NIR) / (SWIR + NIR)
Aerial imagery	1m	2-3 years	The National Agriculture Imagery Program (NAIP)	2018	-

Table 4. Descriptive statistics of predicted air temperature by land cover and the mean differences from the Tree land cover class

Land cover	Count	Area %	Min	Mean	Median	Max	St.Dev.	Difference
Trees	724863	82.8%	34.3	35.8	35.6	38.9	0.6	0.0

Built-up	85920	9.8%	34.5	37.0	37.1	38.9	0.8	1.2
Grassland	53978	6.2%	35.0	36.5	36.3	38.9	0.6	0.7
Barren/sparse vegetation	6585	0.8%	34.4	37.1	37.1	39.0	1.0	1.3
Open Water	3038	0.3%	34.6	35.5	35.4	38.7	0.5	-0.3
Cropland	1370	0.2%	35.0	36.4	36.7	38.7	0.8	0.6
Herbaceous wetland	194	0.0%	34.5	35.3	35.3	36.3	0.3	-0.4

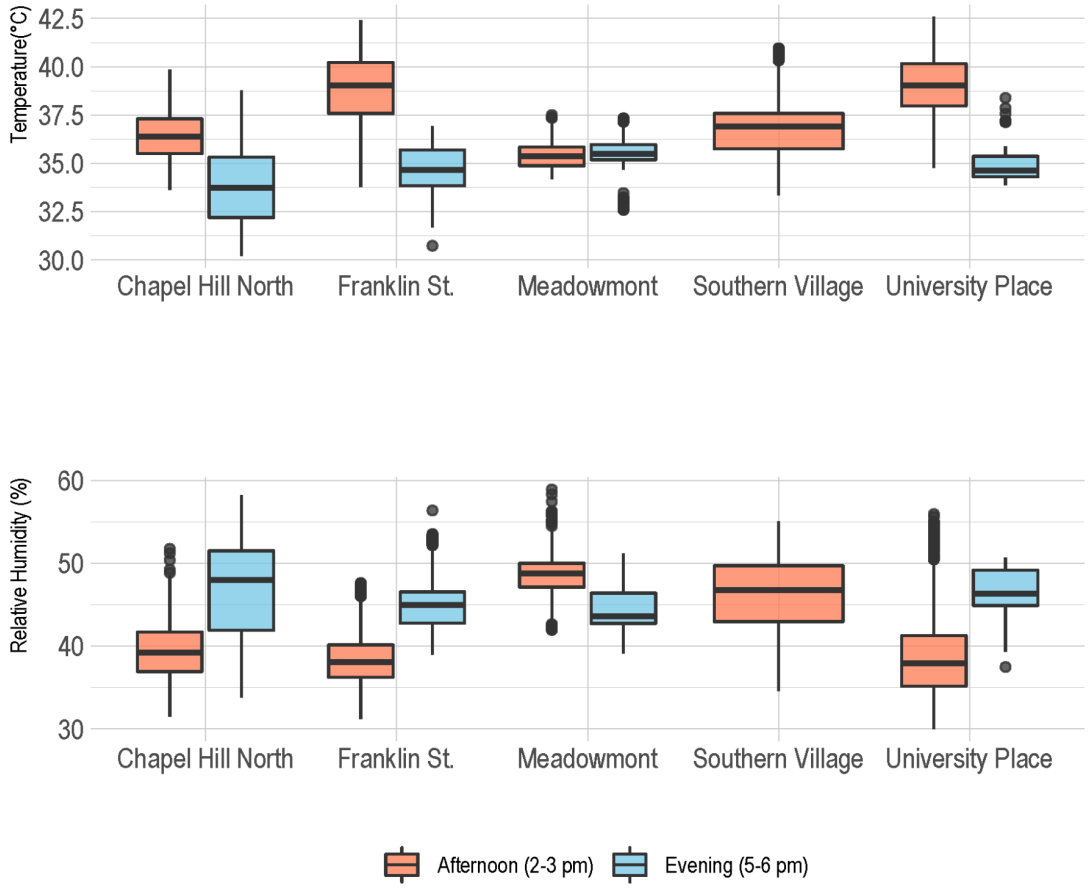

Figure 1. Distributions of air temperature (top panel) and relative humidity (bottom panel) for five neighborhoods mapped in Chapel Hill.

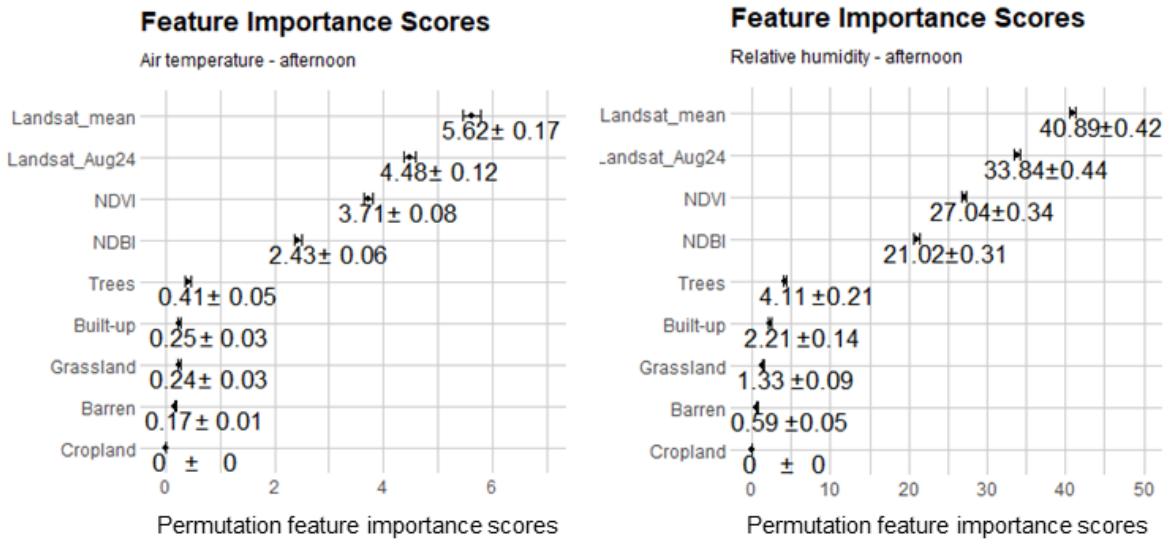

Figure 2. Permutation feature importance scores for temperature (left) and relative humidity (right) models (based on the 50 random training and validation splits)

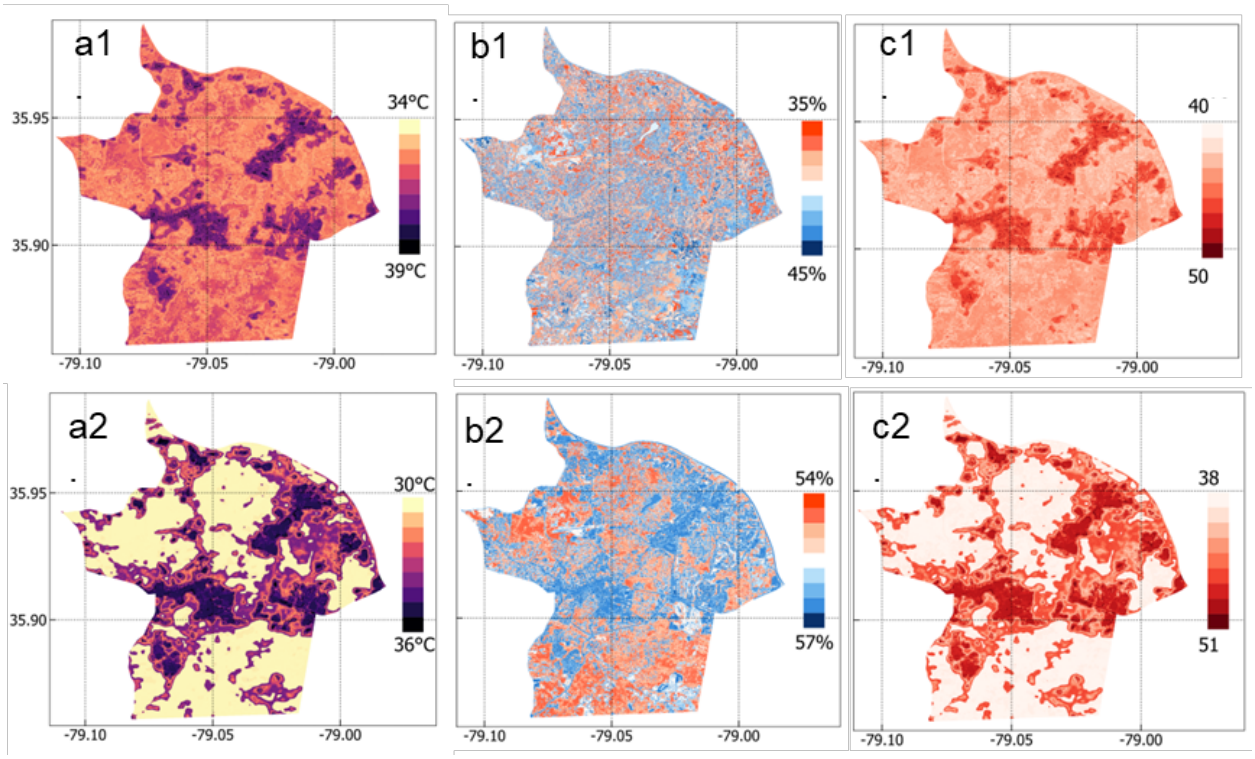

Figure 3. Predicted air temperature, relative humidity, and humidex of the study area (10 meter spatial resolution). a1) predicted air temperature of afternoon session; b1) predicted relative humidity of afternoon session; c1) humidex of afternoon session; a2) predicted air temperature of evening session; b2) predicted relative humidity of evening session; c2) humidex of evening session.

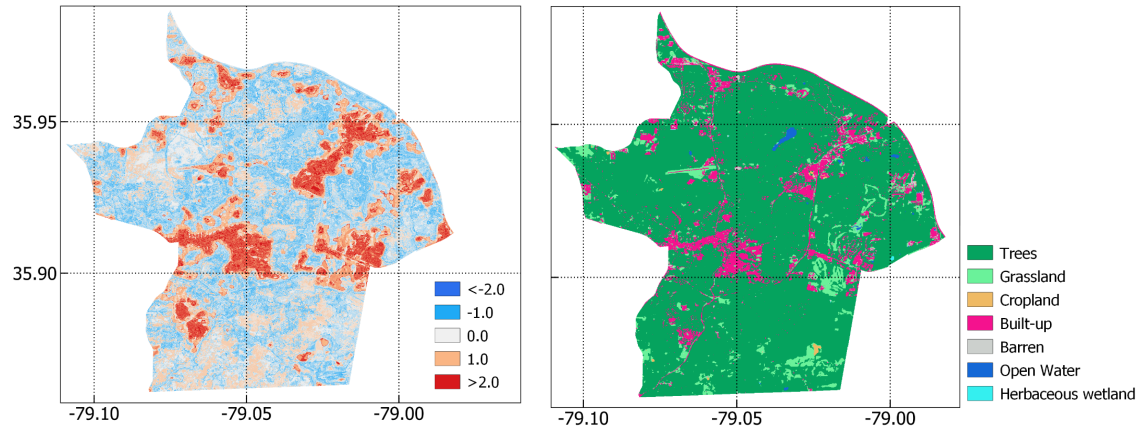

Figure 4. Predicted air temperature anomalies and land cover (10 meter spatial resolution). a) Air temperature differences from mean air temperature of the area covered by trees; b) Land cover types from ESA Worldcover 2020.

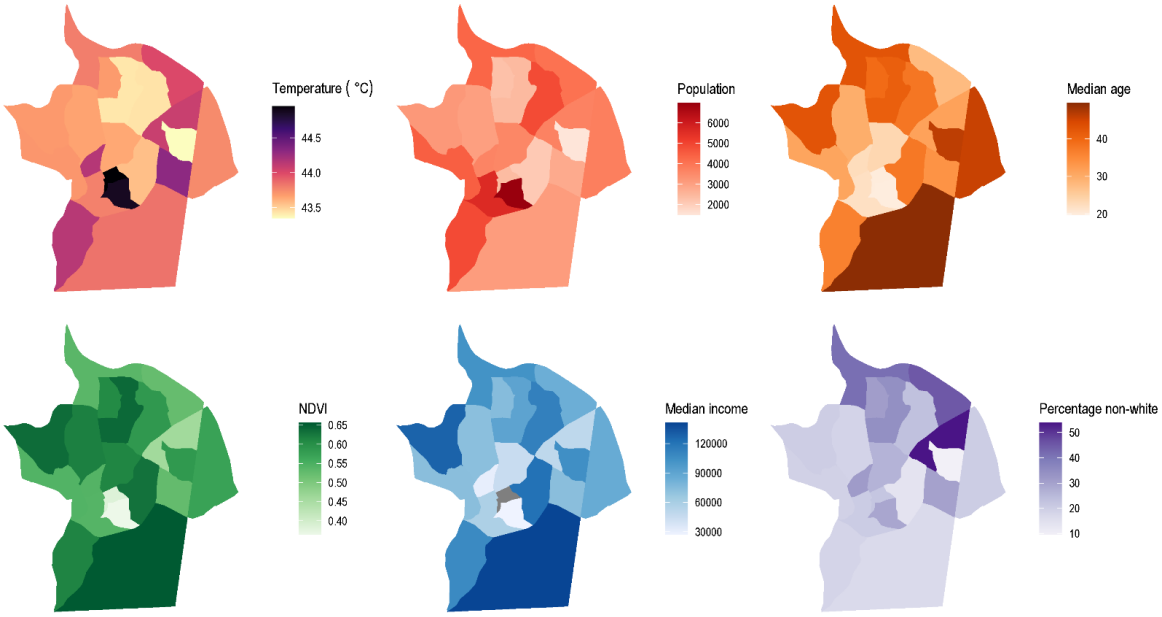

Figure 5. Maps of heat (Humidex), population, median age, greenness (NDVI), median income, and race by census tract in Chapel Hill.

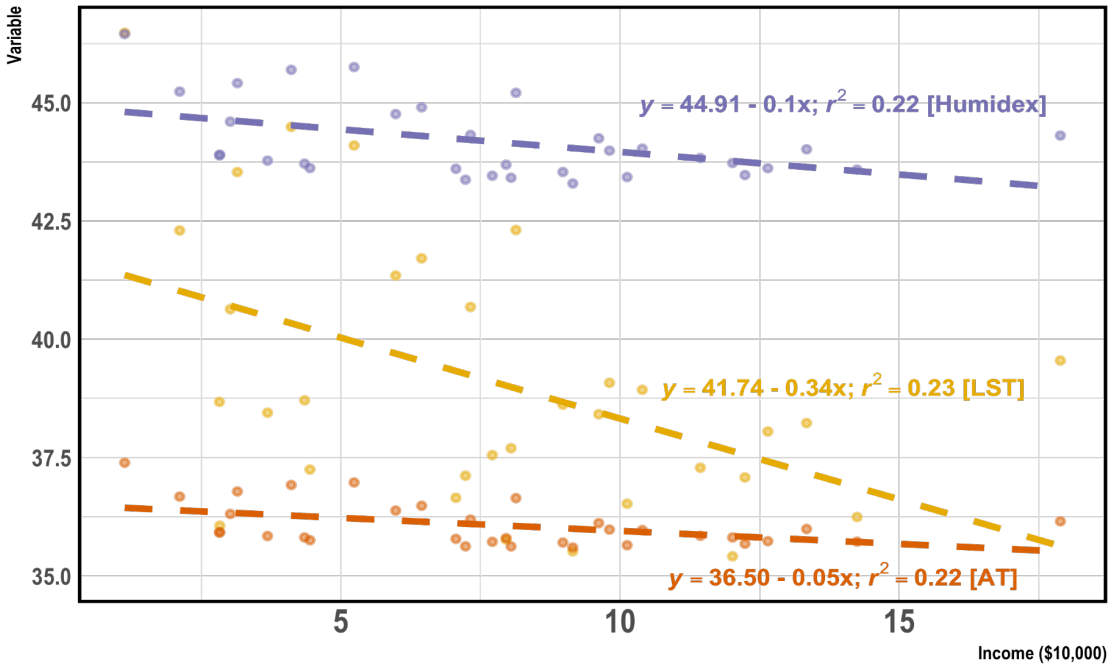

Figure 6. Income versus heat metrics for census block groups during the afternoon in Chapel Hill.